Alexandria Engineering Journal (2023) 66, 475–488

HOSTED BY

Alexandria University

Alexandria Engineering Journal

www.elsevier.com/locate/aej
www.sciencedirect.com

ORIGINAL ARTICLE

One-dimensional ternary conducting polymers blend with 9.26% power conversion efficiency for photovoltaic devices applications

M.H. Abdel-Aziz [a,b,*], H.A. Maddah [a], M. Sh. Zoromba [a,c], Ahmed F. Al-Hossainy [d]

[a] Chemical and Materials Engineering Department, King Abdulaziz University, Rabigh 21911, Saudi Arabia
[b] Chemical Engineering Department, Faculty of Engineering, Alexandria University, Alexandria, Egypt
[c] Chemistry Department, Faculty of Science, 23 December Street, 42521, Port-Said University, Port-Said, Egypt
[d] Chemistry Department, Faculty of Science, New Valley University, 72511 Al-Wadi Al-Gadid, Al-Kharga, Egypt

Received 25 September 2022; revised 23 October 2022; accepted 9 November 2022
Available online 18 November 2022

KEYWORDS

Terpolymers blend;
Polymer thin films;
Bandgap polymer;
TDDFT methods;
Optical properties;
Solar cells

Abstract HCl doped-copolymer of ortho phenylene diamine, meta phenylene diamine, and pyrrole terpolymers blend was synthesized. Physical vapor deposition was used to produce the terpolymer-blended thin films, allowing the creation of the fiber structure at a low deposition rate, with a chamber pressure of 5×10^{-5} mbar and a thickness of 100 ± 2 nm. The produced thin films of terpolymers blend were examined utilizing a combination of theoretical and experimental techniques including TD-DFT/DMol^3, CATSTEP, FT-IR spectrum, XRD, and optical characterizations. According to XRD computations, the terpolymers blend had an average crystallite size of 190 ± 2 nm, while SEM measurements showed that the length of the fibers was ≅ 73 ± 2 μm. The blend of terpolymers displayed an absorbance of 1.83 at 612 nm. Additionally, the blend of terpolymers' indirect/direct bandgap and absorption index was observed with noticeable alterations. The molecular structure optimization and frequency calculations for the crystal models and isolated molecules were carried out using the *materials studio 7.0 tool (TDDFT/DMol^3* and CASTEP). The DFT-Gaussian09W-vibration values closely matched the experimental results in terms of structure and optical characteristics. The application of thin films in polymer solar cell applications looks promising due to the noticeable improvements in optical characteristics.

1. Introduction

The ever-increasing energy consumption is a result of the world's fast-growing population and economy [1]. The massive usage of traditional fossil energy has resulted in significant resource exhaustion and pollution. Searching for alternative renewable energies is one of the most critical options. Solar

* Corresponding author.
E-mail address: mhmousa@alexu.edu.eg (M.H. Abdel-Aziz).
Peer review under responsibility of Faculty of Engineering, Alexandria University.

https://doi.org/10.1016/j.aej.2022.11.013

energy stands out because it is both ecologically beneficial and unrestricted by regional boundaries [2,3]. The solar cell is one of the most efficient ways to utilize solar energy. Currently, solar cell research and development is mostly focused on mature silicon-based solar cells. Even though laboratory efficiency can exceed 25 % [4] the advancement of classic silicon-based solar cells has been hampered by the expensive and difficult production process, and significant energy usage [5]. Polymer solar cells are garnering attention as a prospective use for energy sources due to their combination of flexibility and low-cost manufacture. Attempts have been made over the last two decades to create photosensitive junctions in electrical and optical devices like solar cells by fabricating junction devices with conducting polymers as an active component that can substitute pricey conventional polymers and inorganic semiconductors [6,7]. Conducting polymer thin films have gained a lot of interest in a range of fields due to their mechanical, chemical, and physical properties. This sensor performs best at room temperature, has a high sensitivity, and has quick reaction times. Because of their widespread use as a conducting polymer in the energy industry, conjugate polymers including polyaniline, polythiophene, and polypyrrole have gotten a lot of attention. Polyaniline derivatives have recently been used as homopolymer thin films for polymer solar cell applications, such as poly (ortho phenylenediamine) (PoPDA) microrods with a power conversion efficiency (PCE) of 5.64 % [8], poly (ortho anthranilic acid) microsphere with a PCE of 6.07 % [9], and poly (*ortho*-aminophenol) spherical-like with PCE = 4.28 % [10]. To obtain tunable spectral, morphological, and optical properties, the copolymerization of conjugated monomers (polyaniline derivatives) has been used to meet the characteristics of suitable films for polymer solar cell applications [11]. The copolymer's thin films have been fabricated as heterojunction diode in the polymer solar cells including poly (*para*-nitroaniline- co-aniline) sphere-shaped particles with a PCE of 5.91 % [12], poly (o-phenylenediamine –co– p-toluidine) fibers with a PCE of 6.17 % [13], poly (o-anthranilic acid-*co*– o-aminophenol) microsphere with a PCE of 8.23 % [14]. For the synthesis of conducting polymers, the soft-template technique, which involves the construction of support structures for the growth of 1-Dimensional structures, has been extensively studied. This method is particularly cost-effective for producing polymers with specified topologies. Surfactants as soft templates play an essential role in the polymer structure, which has been characterized as 1-dimensional [15–18] and 2-dimensional structure [19].

The present work aims to prepare the blend of the following three polymers, poly (*ortho*-phenylene diamine) (PoPDA), poly (meta phenylene diamine), and polypyrrole, in the presence of sodium dodecyl sulphate (SDS) in a highly acidic medium utilizing ferric chloride as an oxidizing agent. Enhancing band gap tenability and optical characteristics will enable the mix to be used in more semiconductor applications.

In recent years, polymers with diverse optical properties have been attracted much more attention due to their applications in sensors, optical devices and LEDs. The optical properties can be easily tuned by controlling the amount of dopant nanofillers in to polymer matrix. The important optical parameters of the polymer blend are absorption, absorption coefficient, extinction coefficient and E_g values. In the present work, the UV–visible spectrometer is used to study the above-mentioned optical parameters of synthesized polymer blend. Neoteric TDDFT applications ($DMol^3$ and CASTEP techniques) and the opticalproperties for researching the structure of polymer matrix, stability of copolymer phase, and nanocomposite compounds [20,21] are reviewed. The use of this complete energy-based method for spectroscopic properties estimation and investigation has received little attention. This article discusses the geometrical study and the potential energy of HUMO and LUMO states using a limited programming language [22]. The objective is to demonstrate that the same atomistic modeling techniques may be consistently employed throughout the experimental inquiry to achieve high levels of precision [23]. In either standard-memorizing or ultra-soft formulations, ab initio pseudopotentials are used to represent electron–ion potential. Depending on the reduction of direct energy, the relevant intensity of charge, Kohn–Sham wave functions, and conscience-consistent method are derived. Specifically, applying of density mixing and conjugate techniques are applied. The shape of systems with a finite number of inhabitants could be represented by a strong DFT electron [24]. Copolymer and composite compounds with different k-points used for precise integration of Brillouin zone integration and the plane waves cut-off which supplies the base set size are the much-needed parameters that impact the convergence of the measurements [25].

The literature of polyamine found to be limited in optoelectronic application, so the optical properties of tripolymers attracted our studying attention from which the optoelectronic application can be recommended. The novelty of this study is using HCl doped-copolymer of ortho phenylene diamine, meta phenylene diamine, and pyrrole terpolymers blend as the electrospinning blend in order to improve the tripolymers ability to form blend, in addition of improving the optical stability which is an important factor in optoelectronic applications. First, after forming the (PoPDA), meta phenylene diamine monomer was polymerized on the surface of poly (*ortho*-phenylene diamine) without separating it from the mother solution. Pyrrole monomer was polymerized as well on the surface of both (PoPDA + PmPDA) binary polymers without separation. Thin films have been fabricated from the blend of [P(o&m-PDA + Py)] terpolymers blend via the physical vapor deposition (PVD) method. The size and form of TPTFs were investigated using the data analysis of SEM and XRD. Both the optical and electrical properties of these films are examined.

2. Experimental tools and measurements

2.1. Raw materials

All chemical components were utilized as supplied, with no further processing, except for ortho and meta phenylene diamine and pyrrole. The hydrochloric acid, pyrrole, sodium dodecyl sulphate, and meta & ortho phenylene diamine were all provided by Aldrich. Dimethyl sulfoxide (DMSO), analytical-grade ethanol, and ferric chloride (anhydrous) were provided by Shanghai chemicals. The chitosan is supplied from Marshall Marine Products, located in Erode. Without further purification, these chemicals were used as received. Water was twice distilled before it was used to make reactant solutions and make catalysts. The purity of all used chemicals are presented in Table 1.

Table 1 List of chemicals used, molecular formula, molecular weight, and purity.

Chemical	Molecular Formula	Molecular weight	Purity
m-Phenylenediamine	$C_6H_8N_2$	108.14	99 %
m-Phenylenediamine	$C_6H_8N_2$	108.14	99.5 %
Pyrrole	C_4H_5N	67.09	98 %
Sodium dodecyl sulphate	$C_{12}H_{25}NaO_4S$	288.37	98 %
Hydrochloric acid	HCl	36.46	37 %
Dimethyl sulfoxide	C_2H_6OS	78.13	99.9 %
Ethanol	C_2H_5OH	46.07	99.8 %
Ferric chloride (anhydrous)	$FeCl_3$	162.2	99.99 %

2.2. Synthesis of the terpolymers blend

This was carried out via the following three stages: the first stage started with 1.44 g (0.0133 mol) ortho phenylene diamine (oPDA) (first monomer) was dissolved with a magnetic stirrer in 20 mL of ethanol. To the ethanolic solution, 4 mL of concentrated HCl was added, and then 100 mL of distilled water. The solution had a pH of zero. In 240 mL of $FeCl_3$, 2.88 g of sodium dodecyl sulphate surfactant was dissolved (0.5 M). The oPDA monomer solution was stirred with a magnetic stirrer at 900 rpm for two hours at room temperature while drops of $FeCl_3$ solution were gradually added. oPDA monomer needs around 60 mL ferric chloride solution to completely polymerized. The second stage was carried out as follows: Separately 1.44 g (0.0133 mol) meta phenylene diamine monomer (mPDA) (second monomer) was dissolved in 20 mL ethanol, and it was added drop by drop into the resulting mixture from the first stage (of PoPDA and 180 mL $FeCl_3$ solution) for 1 h. The third stage was carried out as follows: separately 1.85 mL (1.79 g: 0.027) pyrrole was dispersed in 20 mL ethanol and it was added drop by drop into the resulting mixture from the second stage containing PoPDA, PmPDA, and 120 mL $FeCl_3$ solution for 1 h under magnetic stirrer at the previous conditions for an additional hour then it was left overnight. The resulting blend (PoPDA/PmPDA/PPy) was cleaned with distilled water, ethanol, and filtering to get rid of unreacted species and extra ferric chloride solution. Finally, the polymers blend was dried in the oven at 70 °C. The ratios of the monomers and oxidizing agent (oPDA: mPDA: Py: $FeCl_3$ are 1: 1: 2: 9.2. The oxidative polymerization processes can be suggested as illustrated in Fig. 1.

2.3. Synthesis of the terpolymers blend thin film

Physical vapor deposition (PVD) was used with a UNIVEX 250 Leybold (Germany) to deposit the blend thin films, which had a thickness of 100 ± 3 nm, onto a p-Si wafer and ITO/-glass substrate. According to Fig. 2, thin films made of a blend of fibers were formed at a constant vacuum pressure [26]. On the front side of a p-Si wafer substrate, blend thin films were formed using the PVD process before being deposited on pure Au (60 nm). Using magnetron sputtering, the Al- electrode was produced on the back of the p-Si wafer substrate with a thickness of 95 nm. The photoactive region of the 6.25×10^5 m^2 terpolymers blend solar cell Au/n- [blend thin film]/p-Si/Al was developed [27].

3. Results and discussions

3.1. FTIRxxx

FTIR spectroscopy (Vertex 80v powder FT-IR equipment) may be used to identify chemical changes in the mix of polymers (Bruker Optics, Germany). Between 450 and 4000 cm^{-1}, room temperature was used for the experiment. Fig. 3 displays the blend's experimental and calculated IR

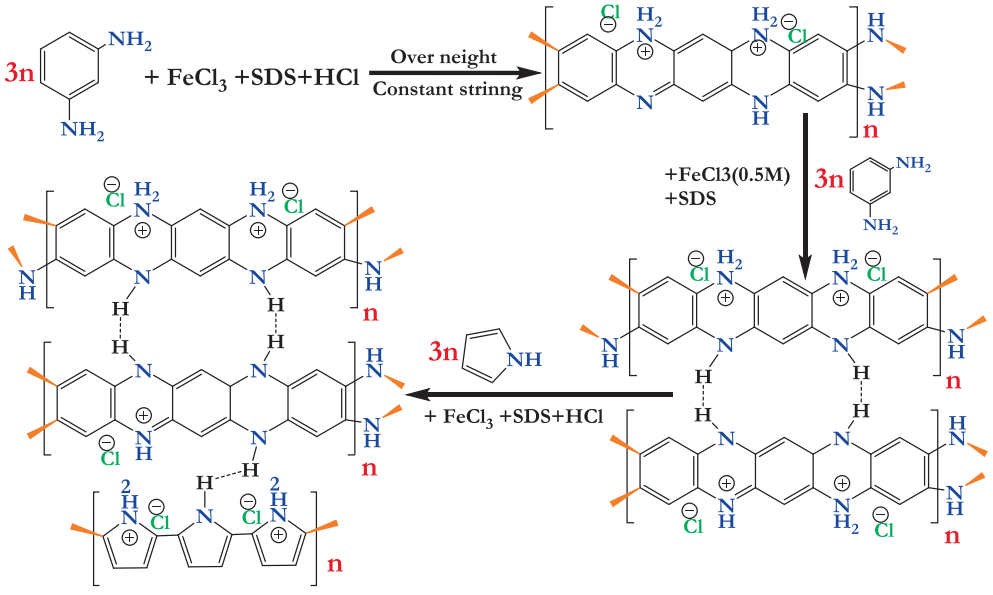

Fig. 1 Suggested oxidative polymerization process for the terpolymers blend.

Fig. 2 Fabrication of terpolymers blend solar cell au/n-[terpolymers blend thin film] /p-si/al.

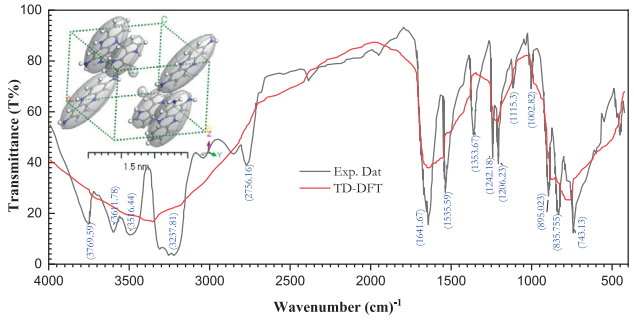

Fig. 3 FTIR spectra and structure of n-[terpolymers mix thin film] and IR modeling with *Gaussian 09 W Software*, DFT/WB97XD, and basis set 6-311G.

spectra. The water molecule's hydroxide group, which is associated with bending, stretching, rocking, and wagging vibrations as shown in the spectrum, is what causes the different bands observed at 1353, 3237, and 743 cm^{-1}. This demonstrates that the terpolymer combination contains water molecules [15,16]. Sharp bands at 743 and 895 cm^{-1} are a result of benzene backbones' out-of-plane-bending vibrations (C—H). The existence of a $–NH_2$ group pending across the blend's backbones may be the cause of the polymer's blend band's location at 3516 cm^{-1}. The –NH stretching, vibration characteristic band for the blend was found at 3237 cm-1. The bands at 1641 cm^{-1} and 1535 cm^{-1} for the o-phenylene diamine and m-phenylene diamine polymers of the blend are evidence of quinonoid and benzenoid stretching vibrations [17,18]. On the other hand, the following unique bands, which are located at 1115 and 1353 cm^{-1}, are caused by the C—N stretching vibration mode in the polypyrrole five-membered ring of the blend. Additionally, the polypyrrole in a blend is frequently identified using the 1115 cm^{-1} and 1002 cm^{-1} bands [19].

3.2. X-ray powder Diffraction (XRD) of terpolymers blend thin films

Fig. 4 illustrates the combined XRD patterns of the terpolymers blend thin film as an experimental part and terpolymers blend as an isolated molecule (simulated part by employed TD-DFT method). The strong peaks at the miller indices (*hkl*) at (022), (013), (112), (130), (052), (025), (035), and (026) for tripolymer are shown in Fig. 4. This intermolecular interference between terpolymers thin film chains may be the cause of these high peaks [28]. *P*-1 relates to the space group's reflection of the triclinic symmetry [29]. This is following the real values of 2, d-spacing, and miller index (*hkl*), as indicated by database code amcsd 0016694. To support the crystal structure of the terpolymers blend thin film shown in this figure, another tiny peak arises at (*hkl*) equates to (121), (033), and (006) [30]. Table 2 showed the crystal device variance, hkl, d-spacing, and full-width at half-maximum (FWHM) (β) of the fabricated thin film's crystalline structure. Fig. 4 prove that the tripolymer has polycrystalline structure with crystal system t*riclinic (anorthic)* with space group *P*-1 (2), cell measurements conditions T = 293 °C and cell unit's parameters are a = 5.40 (7) Å, b = 7.78(2) Å, c = 16.31 (1) Å, α = 96.51°, β = 95.82°, and γ = 90.74°, and volume = 2800 (46) $Å^3$. According to Table 2, the thin film made of a terpolymer blend has an average crystallite size (D_{Av}) of 190.67 nm. Due to the proven correlation between the average crystallite size and the size distribution, the properties of semiconductor materials have been studied for a very long period [31]. A large dispersion spectrum in XRD patterns is based on configurations of atom and crystallite size of particles in unit cells, especially vulnerable to these arrangements [32]. The FWHM (β) and D_{Av} were found to be at $10^0 \leq 2\theta \leq 80^0$. Debye-Scherrer uses Bragg's equation to calculate the interplanar spacing (d-spacing) between the greatest diffraction peaks and D_{Av}:

$$D_{Av} = 0.9\,\lambda/\beta cos\theta \quad (1)$$

where (λ = 0.154 nm), θ is the matching 2θ and the *β* and FWHM (in radians) [33] are recorded in Table 2.

The material studio software's polymorph calculations approach (version 7.0) was used to calculate the PXRD patterns of the polymorphs. As can be seen in the inset of Fig. 4, the integrals over the Brillouin zone were calculated using a 2 × 2 × 1 matrix (polymorph terpolymers blend as isolated molecules). Although there are minor differences in the intensities and locations of several peaks between the experimental and calculated PXRD patterns, we will only focus on the key similarities between them in this section [34]. Along with the characteristics of the devices and data collection techniques, the microstructural characteristics of powder samples can influence the experimental PXRD pattern. This covers the distribution of crystallite sizes, shapes, and orientations. Comparing the observed and anticipated PXRD patterns for

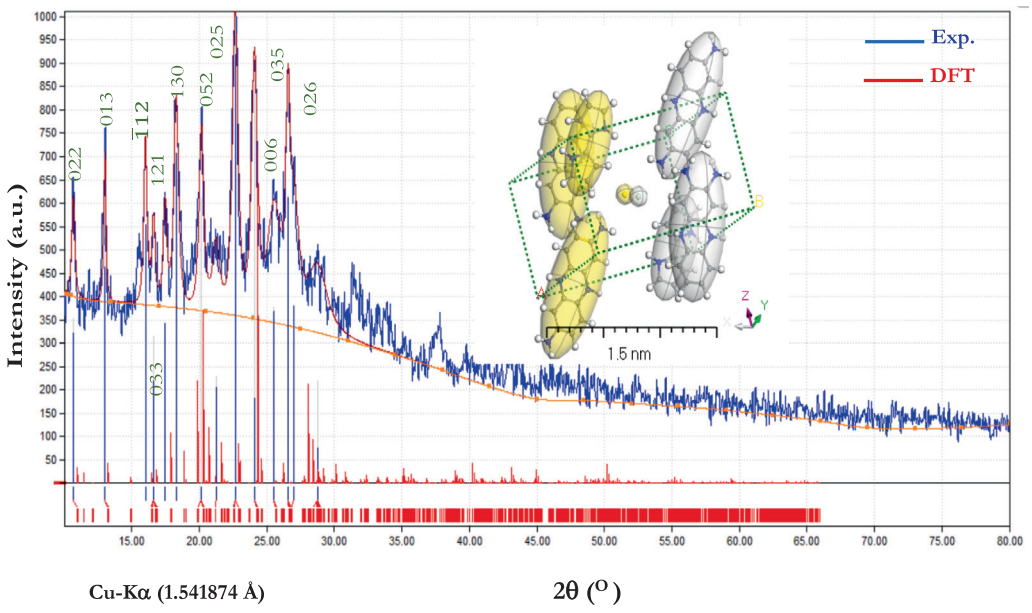

Fig. 4 PXRD patterns for a) the constructed thin-film terpolymers mix and b) the simulated terpolymers blend as an isolated molecule, combined experimental and simulation Figure uses the *Polymorph computation technique* and is a 3D triclinic lattice type.

both polymorphs, it is clear that the synthesized materials' PXRD patterns are accurate [35].

3.3. Geometric study of terpolymers blend as isolated molecule

The M062X/6–31 + G(d,p) calculations were used to find the most stable HOMO and LUMO molecular orbitals in the ground gaseous state, and the results are shown in Fig. 5. The equilibrium state of the molecule is determined by the energy difference between the fragment molecular orbitals theory (FMOs), which is crucial for understanding electrical conductivity and understanding electricity transmission. If the entropy values of isolated chemicals are entirely negative, they are stable [36]. Using the measured FMOs, electrophilic sites in an aromatic molecule can be inferred. The Gutmannat variance technique was applied to the DMB sites to increase the HOMO energy (E_H) when the dimer molecule bonds (DMB) expanded and the bond length decreased [37].

The optimum energy gap (E_g^{Opt}), as well as the reactivity and stability of the molecular system, were taken into consideration when determining these characteristics. The most important variables in determining stability and responsiveness are hardness and softness [38,39]. The energy bandgap, which describes the connection between charge transport in the molecule, and the derived electronegativity equation were shown in Table 3.

$$(\chi) = (E_H + E_L)/2 \tag{2}$$

Table 2 The computing results from the *Refine Version 3.0 Software Program (Kurt Barthelme's and Bob Downs)* for terpolymers blend thin film.

Symmetry	Experimental			Calculated		Difference		FWHM	D_{Av}(nm)
Compound	2θ	d (nm)	*hkl*	2θ	d (nm)	2θ	d (nm)		
Tripolymer	10.67	7.83	022	10.86	7.71	0.19	0.13	0.3450	240.17
Triclinic (anorthic)	12.97	6.51	013	12.96	6.52	−0.01	−0.01	0.3830	210.82
Space group: *P*-1(2)	16.01	5.33	$\bar{1}$ 12	16.01	5.33	0.00	0.00	0.3049	270.50
a = 5.40(7); b = 7.78(2),	16.62	5.14	033	16.64	5.14	0.02	0.01	0.3105	270.03
and c = 16.31 (1) Å;	17.48	4.90	121	17.48	4.90	0.00	0.00	0.3764	220.32
α = 96.51°; γ = 95.82°;	18.31	4.69	130	18.31	4.69	0.00	0.00	0.4611	180.24
β = 90.74°;	20.10	4.28	052	20.10	4.28	0.00	0.00	0.4566	180.47
Rmse [a] = 0.00055457331;	22.62	3.83	025	22.49	3.85	−0.13	−0.02	0.5136	160.49
λ = 1.541838 Å;	24.04	3.61	035	24.00	3.61	−0.04	−0.01	0.4975	170.07
ME [c] = 0.612;	25.65	3.39	006	25.64	3.39	−0.02	0.00	0.6488	130.13
V = 2800 (46)	26.62	3.27	026	26.73	3.26	0.11	0.01	0.8443	100.11
Average									**190.67**

[a] Root mean square error; [b] nm, [c] Machine error.

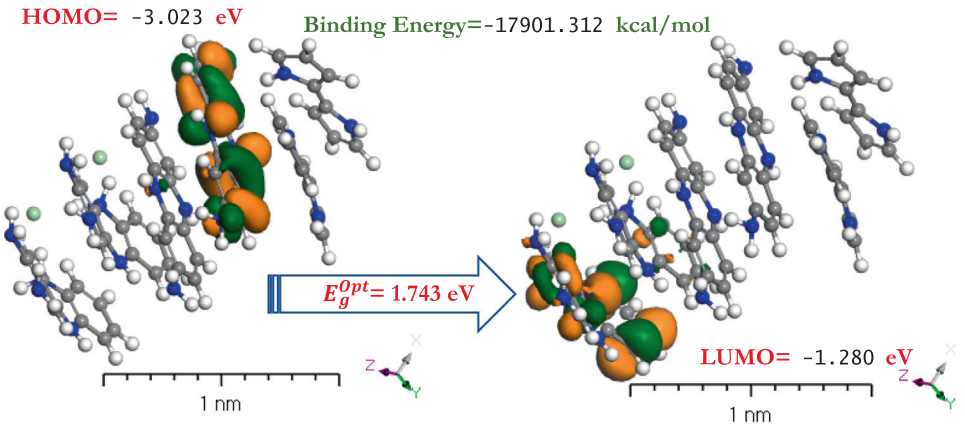

Fig. 5 TD-DFT computations using DMOl^3 method for HOMO and LUMO calculations terpolymers blend thin film dimer as an isolated molecule.

Table 3 Calculated E_H, E_L, global hardness (η), chemical potential (μ), electronegativity (χ), global softness (S), and global electrophilicity index (ω), ΔN_{max} and σ for terpolymers blend as a dimer and an isolated molecule.

Compound	E_H(eV)	E_L(eV)	$\Delta E_g^{Opt.}$	χ (eV)	μ (eV)	η (eV)	S (eV)	ω (eV)	ΔN_{max}	$\sigma(eV)^{-1}$	$(\Delta E_b)^a$
1	−4.889	−2.099	−2.309	3.434	−3.434	1.475	0.339	3.998	2.329	0.678	
Dimer	−4.750	−1.816	−2.934	3.283	−3.283	1.467	0.341	3.674	2.238	0.682	

[1] = terpolymers blend thin film and a) kcal/mol.

The polymer of poly meta phenylenediamine with the p(m-PDA) moiety frequently has the HOMO level, making it a favorable target for nucleophilic attack. Fig. 5 shows that the terpolymer blend dimer's HOMO energy is −3.023 eV in the gaseous state (which is an extremely large value). This value showed that terpolymers merge dimer with high excitation energies and great stability. Contrarily, the lower value energy LUMO = -1.28 eV can be attributed to the ortho phenylenediamine polymer P(o-PDMmore)'s polarizable and softer quinonoid ring, which is concentrated in the gaseous state. Since soft molecules may donate electrons to an acceptor, they are referred to as reactive molecules as opposed to hard molecules. The description that primarily interests us is the measured chemicals index electrophilicity (ω). As it absorbs external electrical charges, the device forecasts energy stability [40,41].

Quantum-chemical computations examined a large number of conformers for the ground state geometry and chose the conformer with the lowest energy, which was supported by the harmonic vibrational frequency. The basis set superposition error was corrected by utilizing the counterpoise correction method BSSE on the dimers binding energies. Terpolymers that combine dimers and single molecules have binding energies of −17901.31 kcal/mol and −8949.69 kcal/-mol, respectively [42].

Using the following formula, the binding energies of dimers ΔE_b were evaluated at the same level of theory:

$$\Delta E_b = E_{dimer} - 2E_{monomer} \quad (3)$$

To further understand the nature of intermolecular interactions, the examined compounds and their dimers were subjected to the TDDFT/DMOl^3 technique [43]. The examined molecule's intermolecular interactions are shown in Fig. 6 and include hydrogen bonds (C—H...HN). The lengths of the hydrogen bond between the dimers of poly pyrrole (PPy), (PPy) and poly m-phenylenediamine P(m-PDA), the dimer of P(m-PDA), P(m-PDA) and poly o-phenylenediamine P(o-PDA) and the dimer of P(o-PDA) are 2.814 Å, 2.531 Å, 2.01 Å, 2.46 Å and 2.514 Å, respectively, in the same order the angle between the tripolymer are 104.89°, 96.03°, 105.81°, 85.12° and 84.26°. On the other hand, the longer centroid lengths of the (PPy) moiety and (P(o-PDM) moiety in the dimer matrix are 9.14 Å and 7.826 Å. The rings of both molecules cannot revolve around the single bonds because the intermolecular distance between the two dimers (the smaller centroid lengths) is less than 3.50 Å. Instead, the rings of the molecules rotate around the centroid point [44]. The dihedral angles (Θ) of P(o&m-PDA + Py) dimers isolated molecule is 4 $46.03^{\circ} \leq \Theta \leq 104.89^{\circ}$, respectively.

3.4. SEM image of terpolymers blend

SEM images of the polymer blend at various magnifications are shown in Fig. 7 (a-c). The PoPDA flakes appear to take the shape of microrods in the SEM pictures. The uniformity of structures produced demonstrates that the synthesized PoPDA involves a high number of uniform microrods. PoPDA has a one-dimensional morphological structure with organized, densely packed fibrous wires or brush. PoPDA microrods had previously been reported as a homopolymer [8]. With the existing image, there is a significant deal of agreement. The creation of PoPDA microrods can be viewed as PoPDA self-assembly including the interactions of intermolec-

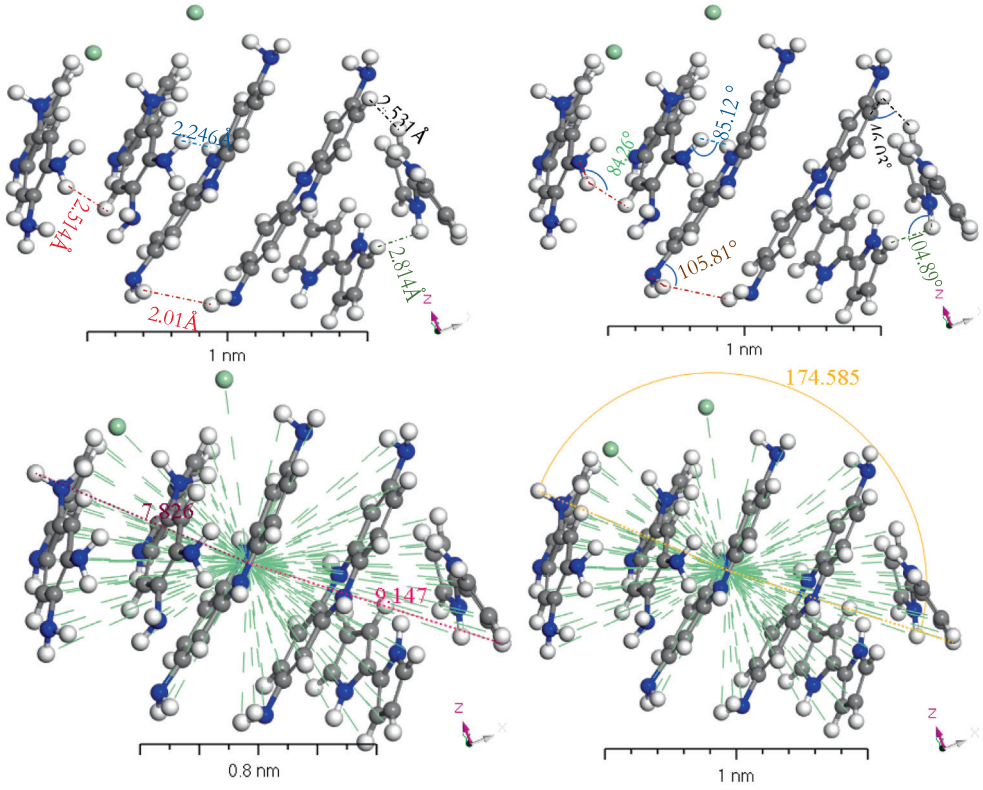

Fig. 6 Stable structures for terpolymers blend dimers in the gas phase, calculated with B3LYP/6-31 + G(d,p).

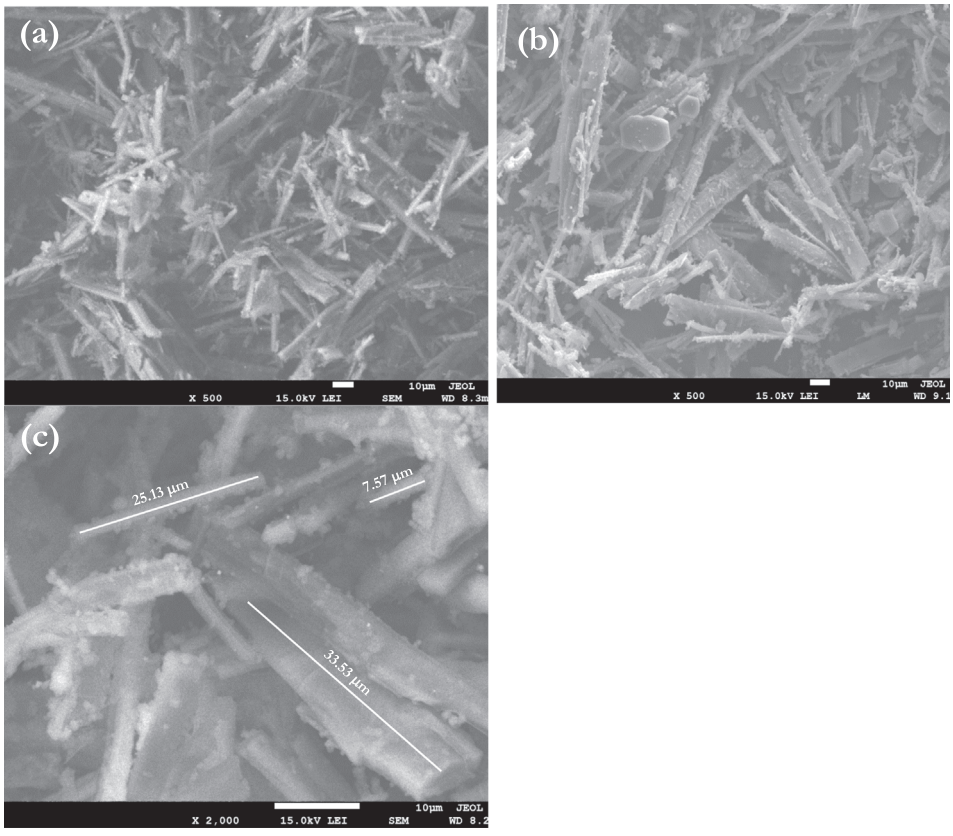

Fig. 7 (a-c). SEM of $[P(o\&m\text{-}PDA + Py)]^{TF}$ at 10 µm magnification with four different locations.

ular π–π and electrostatic repulsion interactions [45], which consider both the intermolecular π–π* interactions with the hydrogen bonds linked between copolymer chains. The SEM image clearly shows PoPDA rods coated with various spherical-shaped particles. The effective deposition of both PmPDA and PPy on the surface of the PoPDA polymer is responsible for the shapes around the PoPDA rods.

3.5. Optical properties of terpolymers blend thin film

Determination of optical transitions and band structure using $[P(o\&m\text{-optical PDA} + Py)]^{TF}$ properties, especially the absorption edge was performed. As a function of photon wavelength (λ) in the UV to the visible area, Fig. 8 compares experimental $[P(o\&m\text{-PDA} + Py)]^{TF}$ and estimated [P(o&m-PDA + Py)] as an isolated molecule in a gaseous state. The experimental optical absorbance spectrum shows two absorption band ends at lower wavelengths, at around 612 nm, because of the interband electronic transition from the highest occupied molecular orbital (HOMO) to the lowest unoccupied molecular orbital (LUMO) (main peak) [46,47]. Using TD-DFT analysis at 900 > λ (nm) > 500, the theoretical optical response of [P(o&m-PDA + Py)] as an isolated molecule was examined. The absorption bands of [P(o&m-PDA + P y)] and $[P(o\&m\text{-PDA} + Py)]^{TF}$ with a thickness of 100 ± 3 nm and produced at 298 K were compared using the TD-DFT/CASTEP data. The primary absorption band edge is shown by the computed optical absorbance spectra to be at 593 nm. These peak intensities are caused by the delocalized π– π* transition [48–51]. At longer wavelengths λ = 705, 751, and 813 nm, both actual and computed data reveal three absorption bands. Furthermore, the experimental main peak is slightly displaced by 30 nm from the corresponding predicted peak in both data sets. As a result, the calculated data can accurately represent the experimental data.

The absorbance spectrum is commonly used to calculate the optical energy bandgap (E_g^{opt}). The dependency α on E_g^{opt} was reported by Eq. (4) in the region of $\alpha > 10^4$ cm^{-1}

$$(\alpha h\upsilon)^m = A(h\upsilon - E_g^{opt}) \tag{4}$$

where m is a transition process power, $m = 2$ for a direct transition, and $m = ø$ for an indirect transition owing to photon absorption. The linear plot of $(\alpha h\nu)^{0.5}$ and $(\alpha h\nu)^2$ vs photon energy (hν) for the experimental $[P(o\&m\text{-PDA} + Py)]^{TF}$ thin film is shown in Fig. 9. For indirect and direct electronic transitions, the intercept of the straight line with the photon energy axis at $(\alpha h\nu)^{0.5}$ and $(\alpha h\nu)^2 = 0$ is used to determine E_g^{opt}. As a result, the indirect $(E_{indir}^{Opt.})$ and direct $(E_{Dir}^{Opt.})$ bandgaps are 1.97 eV and 1.92 eV, respectively. Charge transfer between functional groups of $(E_{Dir}^{Opt.})$ and $(E_{indir}^{Opt.})$ might explain the shift in $E_g^{Opt.}$ [52]. The energy gap between HOMO and LUMO $(\Delta E_g^{Opt.} = (E_H - E_L) = 1.989$ eV determined in the gas phase using the TD-DFT/CASTEP approach is shown in the inset of Fig. 9. As a consequence, the estimated $\Delta E_g^{Opt.}$ may accurately match the experimental results. Large E_g^{Opt} values are useful for applications that need a bigger optical bandgap, such as energy storage applications [53].

To describe optical properties, the refractive index, which is inversely proportional to the optical bandgap, is crucial. In the visible spectrum, transparent materials have low refractive indices [54,55]. For the characterization of optical devices such as optical switches, filters, modulation, and other optoelectronic devices, the refractive index (n) measurement is essential [56]. In this work, the Herve and Vandamme formula, which is given by the following equation, was used to estimate the refractive index [57]:

$$n = \sqrt{1 + (13.6/E_g + 3.47)^2} \tag{5}$$

Refractive index and bandgap energy are denoted by (n) and (E g), respectively. The films' refractive indices range between 1.20 and 1.90. At hν = 2.02 eV, 1.83 is the highest refractive index value that has been measured. Fig. 10(a) illustrates the relationship between the extinction coefficient (k) and the photon energy (hν), where k = αλ/4π and α = the observed absorption. All of the films' obtained spectra had a single absorption band. The electronic transitions including π → π* were given the absorption bands at 2.03 eV. (k-band). For P(o&m-PDA + Py) as an isolated molecule, Fig. 10(b) illustrates the dependency of the refractive index

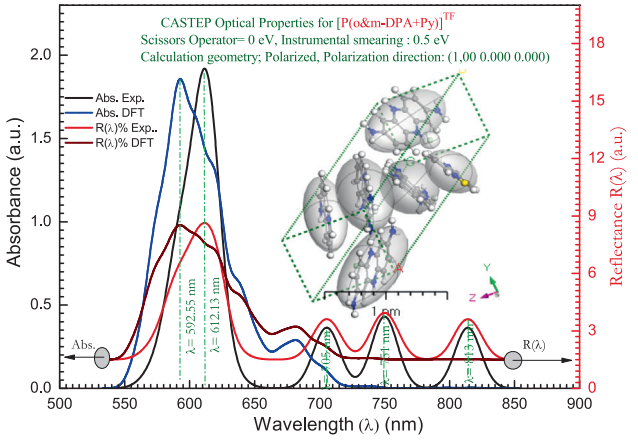

Fig. 8 Experimental and simulated of optical absorbance and reluctance for terpolymers blend thin film and inset Figure is a 3D triclinic lattice type using *Polymorph computation method* for terpolymers blend as isolated molecule.

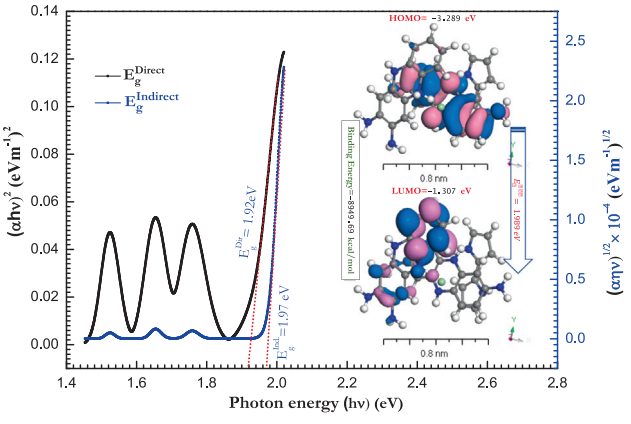

Fig. 9 The link between photon energy and electronic transitions in terpolymer mix thin films. The inset picture shows a schematic depiction of theoretical calculations of the energy gap for the isolated molecule using the TD-DFT/DMol^3 approach.

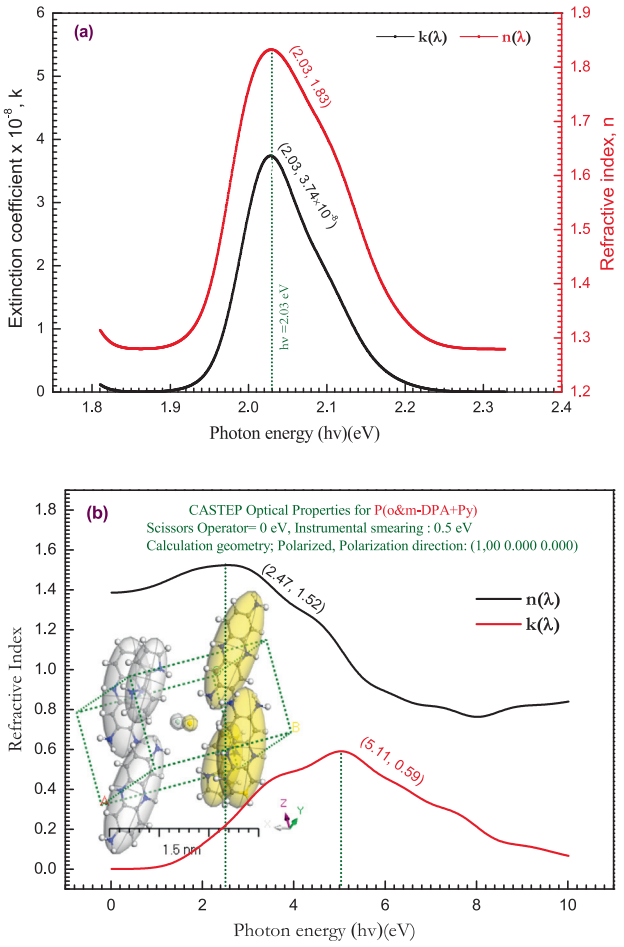

Fig. 10 A) terpolymers' refractive index n(λ) and extinction coefficient k (λ) combine to form thin films. b)The simulated calculation of (n) and (k) was performed by utilizing CASTEP/DFT and the polymorph computation technique, for the terpolymers blend as an isolated molecule. The inset Fig. shows a lattice type: 3D Triclinic.

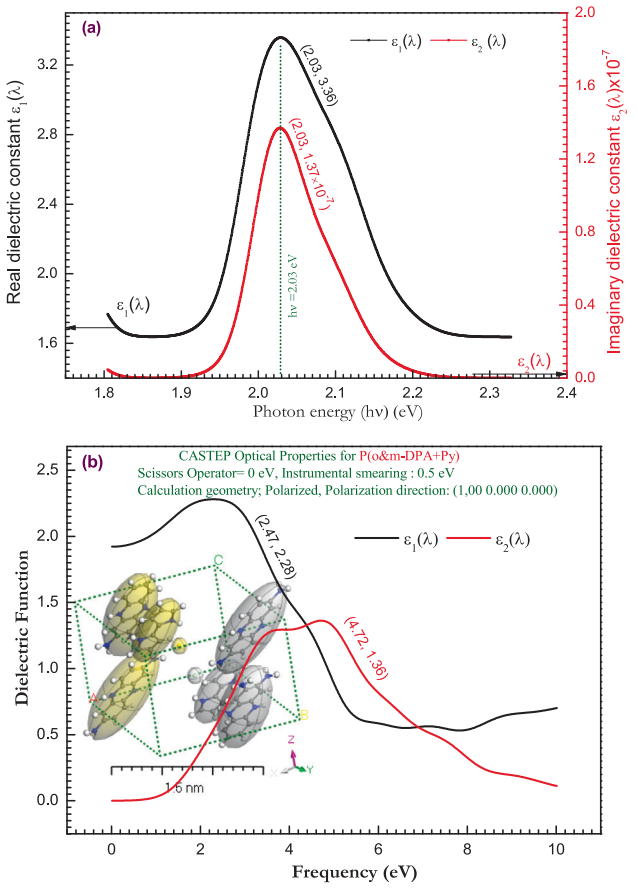

Fig. 11 A) the experimental $\varepsilon_{Re}(\lambda)$ & $\varepsilon_{Imag}(\lambda)$ for terpolymers blend thin film. (b) Simulated $\varepsilon_{Re}(\lambda)$ & $\varepsilon_{Imag}(\lambda)$ for terpolymers blend employing the CASTEP technique, as an isolated state. By applying the polymorph computation approach, the inset Fig is a lattice type: 3D Triclinic.

(n) and extinction coefficient (k) on hν (simulated technique TD-DFT/CASTEP method). Additionally, both data include that the experimental is slightly red-shifted from the corresponding calculated peak. Thus, the computed data can well represent the experimental data [58].

The optical characteristics of a solid substance are described by the complex dielectric constant

$$\varepsilon(w) = \varepsilon_1(w) - i\varepsilon_2(w) \tag{6}$$

The real, $\varepsilon_1(w)$ and imaginary, $\varepsilon_2(w)$ components of the dielectric constant for $[P(o\&m\text{-}PDA + Py)]^{TF}$ thin films are calculated by [59]:

$$\varepsilon_1(\lambda) = n^2(\lambda) - k^2(\lambda) \tag{7}$$

and

$$\varepsilon_2(\lambda) = 2n(\lambda)k(\lambda) \tag{8}$$

Fig. 11 illustrates the fluctuation of $\varepsilon_1(\lambda)$ and $\varepsilon_2(\lambda)$ with the thickness of the films. These statistics demonstrate that the actual component has a greater value than the fictitious part, confirming the thin film's excellent transparency. Additionally, it is noticed from the optical data that the refractive index n, the extinction coefficient k, and the real $\varepsilon_1(\lambda)$ and imaginary $\varepsilon_1(\lambda)$ components of the dielectric constant all exhibit the same behavior as a function of wavelength.

The optical conductivity is given by [60]:

$$Re\sigma_{\alpha\beta}(\omega) = \omega/4\pi Img\varepsilon_{\alpha\beta} \tag{9}$$

Due to the absence of a band gap, the tripolymer blend is an excellent conductor [61]. The development of a blend is motivated by the desire to increase the optical conductivity of polymers. The conductivity of a tripolymer mix is shown in Fig. 12a. In this example, the conductivity of the polymer blend begins at 1.8 eV and ends at 2.40 eV. The optical conductivity of the polymer blend is greater than that of pure o&m-phenylene diamine and polypyrrole [62–64]; the peak maxima for the blend are at 2.66 eV and 3.78 eV, respectively. Fig. 12a illustrates how real and imaginary optical conductivity rises as photon energy increase. The values of real and imaginary optical conductivity reach to maximum observable value $\sigma_1(\omega) = 3.72 \times 10^{-5}$ and $\sigma_1(\omega) = 9.16 \times 10^2$ at $hv = 2.03eV$. Because optical conductivity is connected to absorption spectra, the major edge observed in Fig. 12b (simulated figure resulted for TD-DFT/CASTEP method) corresponds to the previously mentioned optical transitions.

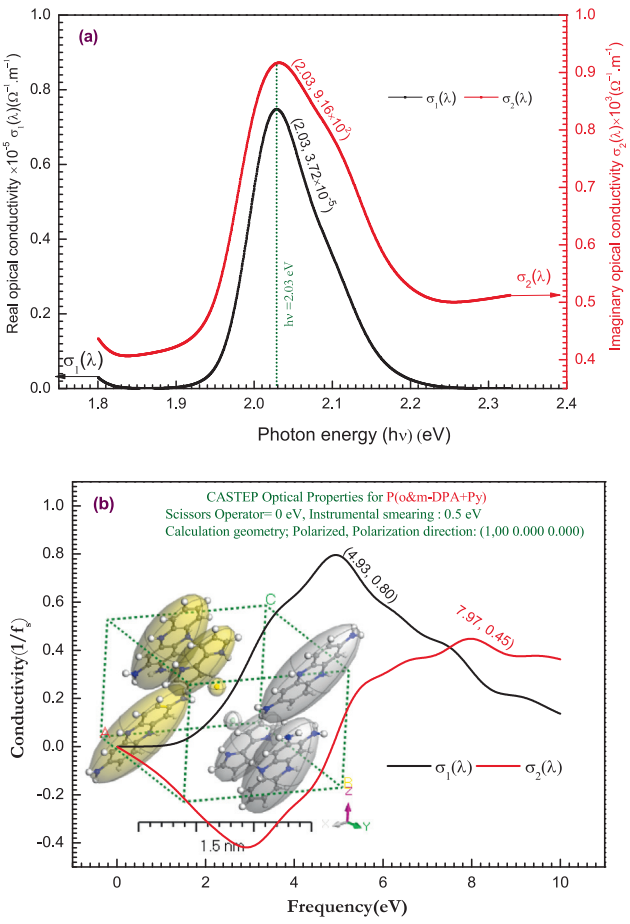

Fig. 12 (a) The experimental $\sigma_1(\lambda)$ and σ_2 $(\lambda)$for terpolymers blend thin film. (b) Simulated $\sigma_1(\lambda)$ and $\sigma_2(\lambda)$ as an isolated state using the CASTEP method.

The Refractive index n(λ) and direct and indirect energy gaps (ΔE) values for all the samples are given in Table 4. Als, the resulted data of dielectric constant ($\varepsilon_{Re}(\lambda)$ and $\varepsilon_{Img}(\lambda)$) and optical conductivity ($\sigma_1(\lambda)$ and σ_2 (λ)) are given in Table 4 for P(o&m-PDA + Py).

3.6. Photoluminescence behavior

Fig. 13a depicts the measured photoluminescence behavior of the $[P(o\&m\text{-}PDA + Py)]^{TF}$ thin film. At wavelengths of 606 nm, the $[P(o\&m\text{-}PDA + Py)]^{TF}$ thin films showed their highest intensities. The emission color coordinates for the solution and thin film were (0.601, 0.0.321) to create blue and cyan emissions, respectively, according to the Commission Internationale de l'Eclairage (CIE). Through the formation of exciplexes and excimers, these π-π interactions lead to the redshift of the emission band [67]. Because the investigated produced copolymer emits white light from a single material and blue and cyan emissions from their solutions, they can be categorized as essential luminogens [68]. This sort of solar cell (Au/$[P(o\&m\text{-}PDA + Py)]^{TF}$ /p-Si/Al) has been used to increase the spectral response by the usage of fluorescent wavelength. As a result, the terpolymer thin film has fully formed in the solid state. Fig. 13b displays the steady fluorescence spectra for the thin film $[P(o\&m\text{-}PDA + Py)]^{TF}$ when adsorbed on quartz slides. This indicates that encapsulation is not as complete as what is seen in the isolated solid state.

3.7. Electrical properties

To study the photovoltaic performance of $[P(o\&m\text{-}PDA + Py)]^{TF}$ produced by oxidative polymerization, a heterojunction structure composed of Au/ $[P(o\&m\text{-}PDA + Py)]^{TF}$/p-Si/Al was manufactured using a conventional-type physical vapor deposition (PVD) process, as seen in Fig. 14. The experimental protocols outline the manufacture and optimization of the gadget. We discovered that the intensity of light illumination had a substantial influence on device performance during the device optimization process. As a result, we conducted a systematic study of the effect of light illumination processing intensity, as discussed below. The current density–voltage (J-V) characteristics of the Au/$P(o\&m\text{-}PDA + Py)^{TF}$/p-Si/Al devices under various illuminations are shown in Fig. 14a and Table 5. This implies that when light is absorbed by the active layer, excitons are produced. These excitons subsequently dissociate into free charge carriers at the barrier, contributing to the photocurrent. On the other hand, it has been observed that light illumination significantly increases the photocurrent in the device. This pattern contains critical information about the electron-hole pairs formed in the junction as a result of the incoming photons. At the junction, the electric field pulled free electrons and holes toward the electrodes along the interface's potential barrier. As shown in Fig. 14, the device has photovoltaic properties, with a high short-circuit photocurrent density *(Jsc)* of 3.96×10^{-3}A/cm^2, an open circuit voltage (V_{oc}) of 78.26×10^{-2} V (when no external load

Table 4 Refractive index n(λ), direct and indirect energy gaps (ΔE) values, dielectric constant ($\varepsilon_{Re}(\lambda)$) and ($\sigma_1(\lambda)$) for P(o&m-PDA + Py) thin films and compassion with a different polymer.

Film composition	Symbols	n(λ)	Dir. Eg	Ind. E_g	ε_{Re} (λ)	($\sigma_1(\lambda)$	Ref.
Poly(o-phenylenediamine) + poly(p-toluidine)	$[PoDA + PpT]^{TF}$	1.64	2.103	1.88	1.35	27.04	[65]
Polyethyleneoxide/Carboxymethyl cellulose	PEO(10 %)/CMC (90 %)	1.79	2.205	4.03	1.45	1.56×10^{-1}	[66]
	PEO(20 %)/CMC (80 %)	1.97	1.85	3.82	1.89	2.31×10^{-1}	
o&m-phenylene diamine, and pyrrole terpolymers blend	P(o&m-PDA + Py)	1.83	1.92	1.97	3.36*	$3.72 \times 10^{-5*}$	PW

Dir. E_g (Direct energy), Indir. E_g (Indiirect energy) and PW (Present work), * Photon energy = 2.03 ev.

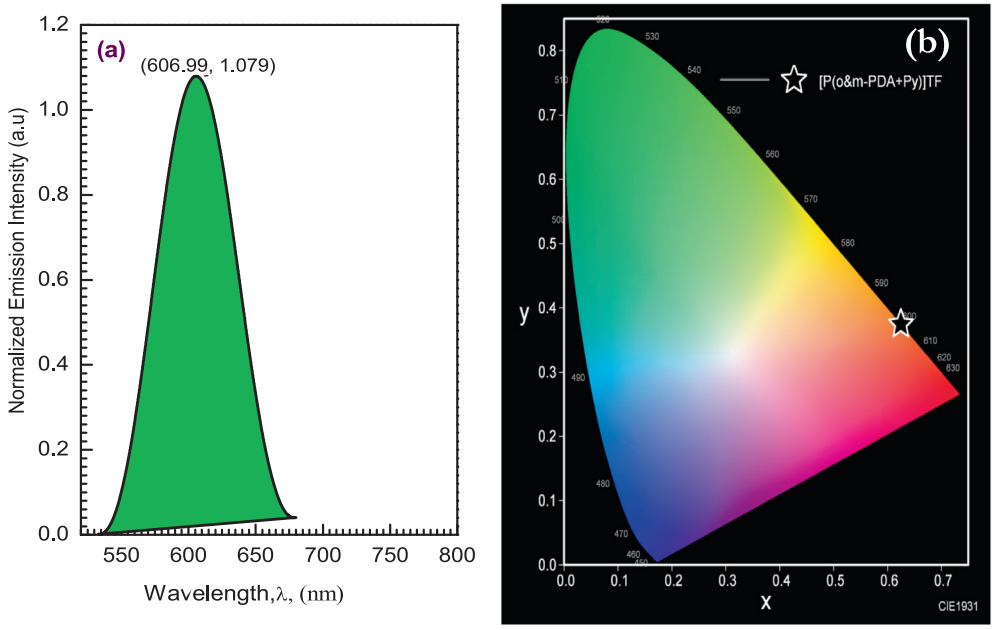

Fig. 13 (a, b) the normalized emission with wavelength and the CIE chromaticity diagrams of the emission colors obtained for terpolymers blend thin films.

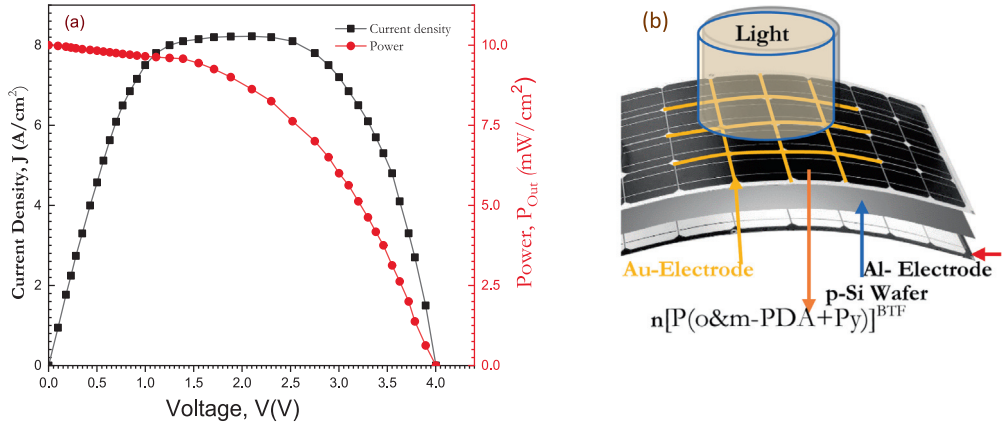

Fig. 14 A) current density–voltage and power-voltage relationships, and b) short-circuit current-power relationships. Include a diagram. [Au/P(o&m-PDA + Py)^{TF}/p-Si/Al] Schematic Diagram heterojunction.

Table 5 Au/P(o&m-PDA + Py)^{TF}/p-Si/Al copolymer device performances under different illumination intensities P_{in}.

Int.[a]	V_m[b]	J_m[c]	V_{oc}[b]	*Power*	*FF%*	*η (PCE)*
30	2.58×10^{-3}	29.48×10^{-3}	42.03×10^{-2}	7.59×10^{-6}	12.13	2.53
50	5.79×10^{-3}	2.91×10^{-3}	45.24×10^{-2}	1.68×10^{-5}	23.27	3.37
70	8.56×10^{-3}	3.12×10^{-3}	47.95×10^{-2}	2.67×10^{-5}	26.90	3.81
90	13.74×10^{-3}	3.24×10^{-3}	50.21×10^{-2}	4.46×10^{-5}	38.58	4.95
110	17.28×10^{-3}	3.42×10^{-2}	53.27×10^{-2}	5.90×10^{-5}	42.78	5.37
130	20.89×10^{-3}	3.61×10^{-2}	57.53×10^{-2}	7.54×10^{-5}	45.53	5.80
150	35.12×10^{-3}	3.96×10^{-2}	78.26×10^{-2}	1.39×10^{-4}	55.99	9.26

a = (W.cm^{-2}), b = Volt, c = (A.cm^{-2}), and d = (mA.cm^{-2}).

is applied, the difference in electrical potential between two terminals of a device.), and a fill factor (FF %) of 55.99 %, as well as the power conversion efficiency (η) of 9.26 %.

In the case of a photovoltaic device, the ratio of the electric energy produced to the energy incident on the cell is 9.26 %. For [Au/ P(o&m-PDA + Py)^{TF}/p-Si/Al] devices, the fluctuation of short-circuit photocurrent (J_{sc}) with incident light intensity (Pin) is shown in Fig. 14b. With an exponent of 0.65, J_{sc} exhibits power law behavior. Bimolecular and monomolecular recombination in ion processes are characterized by s values of 0.5 and 1.0 $(J_{SC} \propto P_{in})^{S}$, respectively [69]. In the case of a continuous distribution of trapping centers, the exponent lies between 0.5 and 1.0. The values of the [P (o&m-PDA + Py)^{TF}/p-Si/Al] diodes show that a continuous trap distribution exists. The longevity of photocarriers is determined by the value of the trap centers.

4. Conclusion

(i) It has been successfully demonstrated that ortho phenylene diamine, meta phenylene diamine, and pyrrole terpolymers can be produced by oxidative polymerization employing ferric chloride as an oxidizing agent. A terpolymer structure with a high density of homogeneous microrods was produced. The desire to improve the optical conductivity of polymers prompted the development of a blend. A terpolymer has a higher conductivity than pure ortho and meta phenylene diamine and poly pyrrole.

(ii) Transparent thin films of terpolymer with a fibrous structure were successfully fabricated using the physical vapor deposition method. The terpolymer has a polycrystalline structure with an average crystallite size of 190.67 nm.

(iii) The high negative value of HOMO demonstrated the terpolymer's durability, whereas the negative value of LUMO demonstrated the availability of electrons.

(iv) Since it produces white light from a single material and blue and cyan emissions from its solutions, the produced terpolymer can be categorized as a key luminogen.

(v) A prospective use for the produced nanocomposite is in photovoltaic technology. Fill factors and power conversion efficiency of a heterojunction constructed of Au/ [P (o&m-PDA + Py)]^{TF}/p-Si/Al were 55.99 % and 9.26 %, respectively, at 150 mW/cm^2.

Declaration of Competing Interest

The authors declare that they have no known competing financial interests or personal relationships that could have appeared to influence the work reported in this paper.

Acknowledgment

This research work was funded by Institutional Fund Projects under grant no. (IFPIP: 219 – 829 – 1442). Therefore, the authors gratefully acknowledge technical and financial support from the Ministry of Education and King Abdulaziz University, DSR, Jeddah, Saudi Arabia.

References

[1] W. Hou, Y. Xiao, G. Han, J.-Y. Lin, The applications of polymers in solar cells: a review, Polymers 11 (2019) 143.
[2] B.K. Sovacool, National context drives concerns, Nat. Energy 3 (10) (2018) 820–821.
[3] Q. Schiermeier, J. Tollefson, T. Scully, A. Witze, O. Morton, Electricity without carbon, Nature 454 (2008) 816–824.
[4] M.A. Green, The path to 25% silicon solar cell efficiency: history of silicon cell evolution, Progr. Photovolt.: Res. Appl. 17 (3) (2009) 183–189.
[5] T.M. Razykov, C.S. Ferekides, D. Morel, E. Stefanakos, H.S. Ullal, H.M. Upadhyaya, Solar photovoltaic electricity: current status and future prospects, Solar Energy 85 (8) (2011) 1580–1608.
[6] Y. Hao, M. Yang, W. Li, X. Qiao, L. Zhang, S. Cai, A photoelectrochemical solar cell based on ZnO/dye/polypyrrole film electrode as photoanode, Solar Energy Mater. Solar Cells 60 (2000) 349–359.
[7] F. Almuntaser, S. Majumder, P.K. Baviskar, J.V. Sali, B. Sankapal, Synthesis and characterization of polypyrrole and its application for solar cell, Appl. Phys. A 123 (2017) 1–8.
[8] M.S. Zoromba, M. Abdel-Aziz, M. Bassyouni, H. Bahaitham, A. Al-Hossainy, Poly (o-phenylenediamine) thin film for organic solar cell applications, J. Solid State Electrochem. 22 (2018) 3673–3687.
[9] A. Al-Hossainy, H.K. Thabet, M.S. Zoromba, A. Ibrahim, Facile synthesis and fabrication of a poly (ortho-anthranilic acid) emeraldine salt thin film for solar cell applications, New J. Chem. 42 (2018) 10386–10395.
[10] A. Al-Hossainy, M.S. Zoromba, M. Abdel-Aziz, M. Bassyouni, A. Attar, M. Zwawi, A. Abd-Elmageed, H. Maddah, A.B. Slimane, Fabrication of heterojunction diode using doped-poly (ortho-aminophenol) for solar cells applications, Physica B: Condensed Matter 566 (2019) 6–16.
[11] S. Jadoun, L. Biswal, U. Riaz, Tuning the optical properties of poly (o-phenylenediamine-co-pyrrole) via template mediated copolymerization, Designed Monomers Polym. 21 (2018) 75–81.
[12] A.F. Al-Hossainy, M.S. Zoromba, Doped-poly (para-nitroaniline-co-aniline): synthesis, semiconductor characteristics, density, functional theory and photoelectric properties, J. Alloys Compounds 789 (2019) 670–683.
[13] M.S. Zoromba, A. Al-Hossainy, Doped poly (o-phenylenediamine-co-p-toluidine) fibers for polymer solar cells applications, Solar Energy 195 (2020) 194–209.
[14] M.S. Zoromba, M. Tashkandi, A. Alshehri, M. Abdel-Aziz, M. Bassyouni, S. Mahmoud, A.B. Slimane, A. Al-Hossainy, Polymer solar cell based on doped o-anthranilic acid and o-aminophenol copolymer, Opt. Mater. 104 (2020) 109947.
[15] M. Li, W. Li, J. Liu, J. Yao, Preparation and characterization of PPy with methyl orange as soft template, J. Mater. Sci.: Mater. Electron. 24 (3) (2013) 906–910.
[16] M. Almasoudi, M.S. Zoromba, M.H. Abdel-Aziz, M. Bassyouni, A. Alshahrie, A.M. Abusorrah, N. Salah, Optimization preparation of one-dimensional polypyrrole nanotubes for enhanced thermoelectric performance, Polymer 228 (2021) 123950.
[17] D. Kopecky, J. Skodova, M. Vrnata, P. Fitl, Polypyrrole micro/nanostructure prepared using azo dyes with different substituents, Adv Mater Phys Chem 02 (04) (2012) 89–91.
[18] N. Baghdadi, M.S. Zoromba, M. Abdel-Aziz, A. Al-Hossainy, M. Bassyouni, N. Salah, One-dimensional nanocomposites based on polypyrrole-carbon nanotubes and their thermoelectric performance, Polymers 13 (2021) 278.
[19] M.S. Zoromba, M.H. Abdel-Aziz, M. Bassyouni, A.M. Abusorrah, A. Attar, N. Baghdadi, N. Salah, Polypyrrole sheets composed of nanoparticles as a promising room

temperature thermo-electric material, Phys. E: Low-Dimens. Syst. Nanostruct. 134 (2021) 114889.
[20] S. Sayyah, H. Mustafa, A. El-Ghandour, A. Aboud, M. Ali, Oxidative Chemical polymerization, kinetic study, characterization and DFT calculations of para-toluidine in acid medium using K2Cr2O7 as oxidizing agent, Int J Adv Res 3 (2015) 266–287.
[21] A.R. Ghazy, M.G. Shalaby, A. Ibrahim, A. ElShaer, Y.-G. Mahmoud, A.F. Al-Hossainy, Synthesis, structural and optical properties of Fungal biosynthesized Cu2O nanoparticles doped Poly methyl methacrylate-co-Acrylonitrile copolymer nanocomposite films using experimental data and TD-DFT/DMOl3 computations, J. Mol. Struct. 1269 (2022) 133776.
[22] I.H. El Azab, A. Ibrahim, M. Abdel El-Moneim, M.S. Zoromba, M.H. Abdel-Aziz, M. Bassyouni, A. Al-Hossainy, A combined experimental and TDDFT-DFT investigation of structural and optical properties of novel pyrazole-1, 2, 3-triazole hybrids as optoelectronic devices, Phase Transitions 94 (2021) 794–814.
[23] T. Hammerschmidt, P. Kratzer, M. Scheffler, Analytic many-body potential for InAs/GaAs surfaces and nanostructures: formation energy of InAs quantum dots, Physical Review B 77 (2008) 235303.
[24] P. Szlachcic, T. Uchacz, M. Gryl, A. Danel, K. Wojtasik, P. Kolek, B. Jarosz, K.M. Stadnicka, Combined XRD and DFT studies towards understanding the impact of intramolecular H-bonding on the reductive cyclization process in pyrazole derivatives, J. Mol. Struct. 1200 (2020) 127087.
[25] M.T. Averbuch-Pouchot, Crystal structure of a tetrameta-polyphosphate: Pb2Cs3 (P4O12)(PO3) 3, Zeitschrift für anorganische und allgemeine Chemie 529 (10) (1985) 143–150.
[26] M.H. Abdel-Aziz, E.Z. El-Ashtoukhy, M. Bassyouni, A.F. Al-Hossainy, E.M. Fawzy, S.M. Abdel-Hamid, M.S.J.C.L. Zoromba, DFT and experimental study on adsorption of dyes on activated carbon prepared from apple leaves, DO I (2020) 1–16.
[27] N. Almutlaq, A. Al-Hossainy, M.S.J.J.o.M.S. Zoromba, Combined experimental and theoretical study, characterization, and nonlinear optical properties of doped-poly (p-nitroaniline-co-o-aminophenol) thin films, 1227 (2021) 129712.
[28] F. Ortéga, M.T. Pope, H.T.J.I.c. Evans, Tungstorhenate heteropolyanions. 2. Synthesis and characterization of enneatungstorhenates (V),-(VI), and-(VII), 36 (1997) 2166-2169.
[29] L. Zhang, P. Xiao, X. Guan, Z. Huang, J. Zhang, X. Bi, Silver-mediated radical coupling reaction of isocyanides and alcohols/phenols in the presence of water: unprecedented hydration and radical coupling reaction sequence, Org. Biomol. Chem. 15 (2017) 1580–1583.
[30] Y. Du, J. Zhang, P. Peng, H. Su, S. Li, S.J.N.J.o.C. Pang, Correction: Synthesis and characterization of three pyrazolate inner diazonium salts: green, powerful and stable primary explosives, 41 (2017) 11422-11422.
[31] Z. Demircioğlu, C.C. Ersanli, S.J.J.o.M.S. Şaşmaz, Spectroscopic, Hirshfeld surface, X-ray diffraction methodologies and local & global chemical activity calculations of 5-(2-methoxy-4-(prop-1-en-1-yl) phenoxy) pyrazine-2, 3-dicarbonitrile, 1181 (2019) 25-37.
[32] A. Al-Hossainy, M.S.J.J.o.M.S. Zoromba, New organic semiconductor thin film derived from p-toluidine monomer, 1156 (2018) 83-90.
[33] A.F. Al-Hossainy, A.J.M.S.i.S.P. Ibrahim, Structural, optical dispersion and dielectric properties of novel chromium nickel organic crystalline semiconductors, 38 (2015) 13-23.
[34] S.A. Mahmoud, A.A. Al-Dumiri, A.F.J.V. Al-Hossainy, Combined experimental and DFT-TDDFT computational studies of doped [PoDA + PpT/ZrO2] C nanofiber composites and its applications, 182 (2020) 109777.
[35] S. Tariq, M. Khalid, A.R. Raza, S.L. Rubab, S.F. de Alcântara Morais, M.U. Khan, M.N. Tahir, A.A.C.J.J.o.M.S. Braga, Experimental and computational investigations of new indole derivatives: A combined spectroscopic, SC-XRD, DFT/TD-DFT and QTAIM analysis, 1207 (2020) 127803.
[36] M. Miar, A. Shiroudi, K. Pourshamsian, A.R. Oliaey, F.J.J.o.C. R. Hatamjafari, Theoretical investigations on the HOMO–LUMO gap and global reactivity descriptor studies, natural bond orbital, and nucleus-independent chemical shifts analyses of 3-phenylbenzo [d] thiazole-2 (3 H)-imine and its para-substituted derivatives: Solvent and substituent effects, 45 (2021) 147-158.
[37] R. Srivastava, L. Sinha, M. Karabacak, O. Prasad, S. Pathak, A. Asiri, M.J.S.A.P.A.M. Cinar, B. Spectroscopy, Spectral features, electric properties, NBO analysis and reactivity descriptors of 2-(2-Benzothiazolylthio)-Ethanol: Combined experimental and DFT studies, 136 (2015) 1205-1215.
[38] N. Almutlaq, A.J.C.I. Al-Hossainy, Novel synthesis, structure characterization, DFT and investigation of the optical properties of diphenylphosphine compound/zinc oxide [DPPB + ZnO] C nanocomposite thin film, 28 (2021) 879-904.
[39] K. Zare, N. Shadmani, E.J.J.o.N.i.C. Pournamdari, DFT/NBO study of Nanotube and Calixarene with anti-cancer drug, 3 (2013) 1-6.
[40] M. Ahmed, T. Zewail, E.Z. El-Ashtoukhy, H. Farag, I. El Azab, F. Albatati, A. Al-Hossainy, M.S. Zoromba, M. Abdel-Aziz, Enhancement of heavy metals recovery from aqueous solutions by cementation on a rotating cylinder using a stationary wiper, J. Ind. Eng. Chem. 97 (2021) 460–465.
[41] B.-H. Jeong, E.M. Hoek, Y. Yan, A. Subramani, X. Huang, G. Hurwitz, A.K. Ghosh, A.J.J.o.m.s. Jawor, Interfacial polymerization of thin film nanocomposites: a new concept for reverse osmosis membranes, 294 (2007) 1-7.
[42] M.J. Mayor-Lopez, J.J.C.p.l. Weber, DFT calculations of the binding energy of metallocenes, 281 (1997) 226-232.
[43] S. Grimme, J. Antony, S. Ehrlich, H.J.T.J.o.c.p. Krieg, A consistent and accurate ab initio parametrization of density functional dispersion correction (DFT-D) for the 94 elements H-Pu, 132 (2010) 154104.
[44] Q. Li, Z.J.A.s. Li, The strong light-emission materials in the aggregated state: what happens from a single molecule to the collective group, 4 (2017) 1600484.
[45] X. Sun, S. Dong, E. Wang, Formation of o-phenylenediamine oligomers and their self-assembly into one-dimensional structures in aqueous medium, Macromol. Rapid Commun. 26 (2005) 1504–1508.
[46] M. El-Nahass, Z. El-Gohary, H. Soliman, Structural and optical studies of thermally evaporated CoPc thin films, Optics Laser Technol. 35 (2003) 523–531.
[47] M. Abd El-Aal, R.T. Mogharbel, A. Ibrahim, N. Almutlaq, M. S. Zoromba, A.F. Al-Hossainy, S.M. Ibrahim, Synthesis, characterization, and photosensitizer applications for dye-based on ZrO2-acriflavine nanocomposite thin film [ZrO2 + ACF] C, J. Mol. Struct. (2022) 131827.
[48] A. Badr, A. El-Amin, A. Al-Hossainy, Synthesis and optical properties for crystals of a novel organic semiconductor [Ni (Cl) 2 {(Ph 2P) 2CHC (R 1R 2) NHNH 2}], Eur. Phys. J. B-Condens. Matter Complex Syst. 53 (2006) 439–448.
[49] A. Badr, A. El-Amin, A. Al-Hossainy, Elucidation of charge transport and optical parameters in the newly 1CR-dppm organic crystalline semiconductors, J. Phys. Chem. C 112 (2008) 14188–14195.
[50] M. Tolba, A.F. Al-Hossainy, A.M. Kamal Eldean, O. Younis, From blue to green photoluminescence: design, synthesis, and DFT calculations of heterocyclic compounds containing chromenothienopyrimidine moiety, Asian J. Org. Chem. (2022).
[51] H. Sami, O. Younis, Y. Maruoka, K. Yamaguchi, K. Siddhant, K. Hisano, O. Tsutsumi, Negative thermal quenching of

photoluminescence from liquid-crystalline molecules in condensed phases, Crystals 11 (2021) 1555.
[52] A.F. Al-Hossainy, M.S. Zoromba, Novel synthesis, characterization and TDD-DFT computations for ZrO2-bromothymol blue nanocomposite thin film [ZrO2+ BTB] C and its application, DOI (2021).
[53] Z. Zhang, Y. Lai, Z. Zhang, K. Zhang, J. Li, Al2O3-coated porous separator for enhanced electrochemical performance of lithium sulfur batteries, Electrochimica Acta 129 (2014) 55–61.
[54] E. Ozugurlu, Estimation of structural and optical parameters of (Mg, B) co-doped ZnO nanoparticles, Gazi University J. Sci. 34 (2021) 529–548.
[55] G. Demircan, S. Yalcin, K. Alivi, G. Ceyhan, A. Acikgoz, M.V. Balak, B. Aktas, R. Das, The effect of Co and Mn Co-doping on structural and optical properties of ZnO thin films, Optical Materials 126 (2022) 112163.
[56] A. Alsaad, Q.M. Al-Bataineh, A. Ahmad, Z. Albataineh, A. Telfah, Optical band gap and refractive index dispersion parameters of boron-doped ZnO thin films: A novel derived mathematical model from the experimental transmission spectra, Optik 211 (2020) 164641.
[57] P. Herve, L. Vandamme, General relation between refractive index and energy gap in semiconductors, Infrared Phys. Technol. 35 (1994) 609–615.
[58] S.M. Ibrahim, A. Bourezgui, A.F. Al-Hossainy, Novel synthesis, DFT and investigation of the optical and electrical properties of carboxymethyl cellulose/thiobarbituric acid/copper oxide [CMC + TBA/CuO] C nanocomposite film, J. Polym. Res. 27 (2020) 1–18.
[59] S.M. Ibrahim, A. Bourezgui, A.A.I. Abd-Elmageed, I. Kacem, A.F. Al-Hossainy, Structural and optical characterization of novel [ZnKCMC] TF for optoelectronic device applications, J. Mater. Sci.: Mater. Electron. 31 (11) (2020) 8690–8704.
[60] A. Al-Hossainy, M. Bassyouni, M.S. Zoromba, Elucidation of electrical and optical parameters of poly (o-anthranilic acid)-poly (o-amino phenol)/copper oxide nanocomposites thin films, J. Inorg. Org. Polym. Mater. 28 (2018) 2572–2583.
[61] Y. Yao, M.A. Kats, R. Shankar, Y. Song, J. Kong, M. Loncar, F. Capasso, Wide wavelength tuning of optical antennas on graphene with nanosecond response time, Nano Lett. 14 (2014) 214–219.
[62] M.S. Zoromba, A. Alshehri, A. Al-Hossainy, M. Abdel-Aziz, Doped-poly (anthranilic acid-co-o-phenylene diamine) thin film for optoelectronic applications, Opt. Mater. 111 (2021) 110621.
[63] M.S. Zoromba, A. Al-Hossainy, S. Mahmoud, A. Bourezgui, E. Shaaban, Improvement of the thermal stability and optical properties for poly (ortho phenylene diamine) using soft templates, J. Mol. Struct. 1221 (2020) 128792.
[64] A. Bourezgui, A.F. Al-Hossainy, I.H. El Azab, F. Alresheedi, S. A. Mahmoud, M. Bassyouni, M.H. Abdel-Aziz, M.S. Zoromba, Combined experimental and TDDFT computations for the structural and optical properties for poly (ortho phenylene diamine) thin film with different surfactants, J. Mater. Sci.: Mater. Electron. 32 (5) (2021) 5489–5503.
[65] S.A. Mahmoud, A.A. Al-Dumiri, A.F. Al-Hossainy, Combined experimental and DFT-TDDFT computational studies of doped [PoDA+ PpT/ZrO2] C nanofiber composites and its applications, Vacuum 182 (2020) 109777.
[66] A. Rajeh, M.A. Morsi, I.S. Elashmawi, Enhancement of spectroscopic, thermal, electrical and morphological properties of polyethylene oxide/carboxymethyl cellulose blends: combined FT-IR/DFT, Vacuum 159 (2019) 430–440.
[67] F.M. Winnik, Photophysics of preassociated pyrenes in aqueous polymer solutions and in other organized media, Chem. Rev. 93 (1993) 587–614.
[68] Q. Zeng, Z. Li, Y. Dong, A. Qin, Y. Hong, L. Ji, Z. Zhu, C.K. Jim, G. Yu, Q. Li, Fluorescence enhancements of benzene-cored luminophors by restricted intramolecular rotations: AIE and AIEE effects, Chem. Commun., DO I (2007) 70–72.
[69] A. Attar, R.D. Alharthy, M. Zwawi, M. Algarni, F. Albatati, M. Bassyouni, M.H. Abdel-Aziz, M.S. Zoromba, A.F. Al-Hossainy, Fabrication, characterization, TD-DFT, optical and electrical properties of poly (aniline–co–para nitroaniline)/ZrO2 composite for solar cell applications, J. Ind. Eng. Chem. 109 (2022) 230–244.